





Argon doped pellets for fast and efficient radiative power removal in ASDEX Upgrade

A. Kallenbach^{1,*} , P.T. Lang¹, M. Bernert¹, R. Dux¹, T. Eberl¹, T. Gleiter^{1,2}, R.M. McDermott¹ , C. Piccinni¹, B. Ploeckl¹ , V. Rohde¹, A. Zito¹  and the ASDEX Upgrade Team^a

¹ Max Planck Institute for Plasma Physics, D-85748 Garching, Germany

² Physik-Department E28, Technische Universität München, 85747 Garching, Germany

E-mail: arne.kallenbach@ipp.mpg.de

Received 10 May 2022, revised 1 July 2022

Accepted for publication 10 August 2022

Published 30 August 2022



CrossMark

Abstract


Argon doped deuterium pellets with about 1 per mille Ar atomic fraction have been injected into ASDEX Upgrade H-mode discharges and demonstrate fast and efficient power removal from the outer plasma region. Bolometer views directly on the pellet and in its very close vicinity observe a strong, non-toroidally symmetric radiation pattern on a fast, sub-ms time scale. This pattern is explained by the ionisation process of the delivered Ar neutrals, leading to non-coronal radiation by intermediate ionisation stages until the equilibrium He like stage is reached. Subsequently, a toroidally symmetric radiation increase is observed with a fast initial decay time of about 20 ms consistent with the radial particle transport time scale for a source located in the outer plasma. In the following, a radiation pattern related to Ar recycling develops comparable to the pattern observed with Ar midplane gas puffing which decays with the Ar divertor pumping time of about 200 ms. The energy radiated around each pellet is described by the radiative potential of Ar evaluated for non-coronal conditions with the ablation time as the relevant time scale. A factor 4 too low radiated energy is obtained by this simple model, which could be explained by stronger deviations from corona equilibrium and plasma parameter variations in the vicinity of the pellet. Injection of Ar-doped pellets into a no-ELM quasi-continuous exhaust H-mode discharge showed no triggering of ELMs by the pellet. Advantages of the pellet seeding scheme are the faster reaction time of the radiation compared to gas puffing, which may be important to counter-act transient re-attachment in ITER or in a reactor and an elevated radiative efficiency in the outer core plasma due to non-corona effects.

Keywords: tokamak, ASDEX Upgrade, argon doped pellets, radiative cooling

(Some figures may appear in colour only in the online journal)

* Author to whom any correspondence should be addressed.

^a See Stroth *et al* 2022 (<https://doi.org/10.1088/1741-4326/ac207f>) for the ASDEX Upgrade Team.

 Original content from this work may be used under the terms of the [Creative Commons Attribution 4.0 licence](https://creativecommons.org/licenses/by/4.0/). Any further distribution of this work must maintain attribution to the author(s) and the title of the work, journal citation and DOI.

1. Introduction

Radiative power removal from the pedestal top or slightly further inward will be a key element for divertor protection and possibly also ELM avoidance in ITER and DEMO [1]. Optimisation goals are a low core fuel dilution per radiated power and a quick reaction time, which is required to counter-act a possible transient re-attachment of the divertor [2, 3]. Argon doped deuterium pellets have been injected into ASDEX Upgrade to assess the radiative cooling scheme and to estimate the radiated energy per pellet, following the validation of the doping scheme using xenon [4]. Advantages of the doped pellet injection compared to impurity gas puffing are demonstrated in this paper.

2. Injection of Ar doped pellets in ASDEX Upgrade

Ar doped deuterium pellets were injected into AUG with the centrifuge injector [5] following procedures previously developed for N [6] and Xe [4] doping. The pellets have a cubic shape with about 2 mm edge lengths and contain about 0.1 atom % Ar, which is an order of magnitude lower compared to the gas concentration before freezing, resulting in about 3.6×10^{20} D atoms and about 3.6×10^{17} Ar atoms per pellet. The pure D reference pellets had 3.6×10^{20} D atoms as well. The pellet injection speed was 550 m s^{-1} and injection rates used were 23, 35 and 70 Hz. The target plasma was under ELMy H-mode conditions, resulting in ELM triggering by the pellets in case that sufficient time had elapsed since the previous pellet [7]. Figure 1 shows video images of doped and non-doped pellets. Within individual scatter, no difference is seen in the visible light range.

Figure 2 shows time traces of two discharges that differ only in the gas and pellet fueling. In the first, # 40106 shown on the left, Ar was fueled from a gas valve located in the outer midplane. The Ar puff rate was in feedback control for a steady decrease of the power entering the divertor from 9 MW to 8 MW [8], leading to a continuous rise in Ar radiation. In addition, pure D pellets were injected to obtain similar plasma parameters in comparison to the discharge with Ar doped D pellets. The second discharge, # 40109 shown on the right, injected Ar doped D pellets with different frequencies. The pellets cause an instantaneous plasma Ar fueling which decays quickly to a level which is determined by recycling. The highest pellet frequency corresponds to an argon fueling rate of 4.5×10^{20} electrons s^{-1} . Apart from the immediate rise of the He-like Ar density in the plasma after pellet injection, the Ar recycling level, which is related to the Ar pumping speed leading to a global Ar confinement time τ^* of 0.2–0.3 s [9], is comparable for pellets and gas valve when the absolute fueling rate is taken into account. This similarity is seen in figure 2 comparing $t = 5 \text{ s}$ in the gas valve fuelled discharge with $t = 5.5 \text{ s}$ with pellet fuelling, having similar Ar particle input. A He-like Ar density of $1.5 \times 10^{16} \text{ m}^{-3}$ corresponds

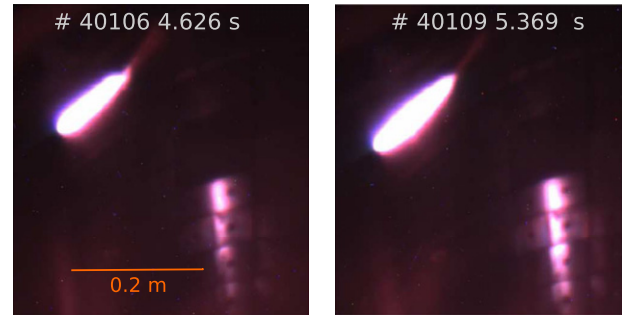


Figure 1. Visible survey camera pictures of the ablating pellets without (left) and with (right) Ar doping. While the pellets appear similar in the visible spectral range, which is dominated by the D_α line, the doped pellet is more than an order of magnitude brighter in the VUV range, as shown in figure 4. The pellets are injected from the upper high field side, the geometry is shown in figure 3. The bright structure on the lower right is the reflected pellet radiation from the inner heat shield.

to an Ar concentration of 0.02%, so Ar is in trace levels and does not strongly effect the global radiation energy balance. It should be noted that the first pellets shown in figure 2 may have a slightly enhanced Ar content due to inhomogeneities of the ice rod.

3. Energy radiated by a pellet

The pellet ablation is observed by fast, but uncalibrated AXUV bolometers and slow, but calibrated foil bolometers [11]. The foil bolometers measure the emitted energy correctly despite the strong temporal smoothing. Figure 3 shows the foil and AXUV bolometer lines of sight that are relevant for the Ar pellet radiation analysis. Full time dependence is obtained from the AXUV diodes. The foil bolometers measure the radiated energy, but the spatial overlap of the emitting region and the bolometer chords introduces an uncertainty, in particular due to the not well known toroidal extension of the radiating Ar layer.

The AXUV diodes allow fast tracking of the pellet emitted power (in relative units). Figure 4 shows fast AXUV diode measurements tracking the pellet along its path from chord to chord. Some track bending/acceleration of the pellet is present [12, 13], leading to the propagation of the pellet front through the DVC lines of sight appearing a bit faster than its nominal speed of 550 m s^{-1} . Ablation completes at a radius $\rho_{\text{pol}} \approx 0.6$. An ablation duration of typically 0.1 ms is seen in individual AXUV chords. Due to the fast timescale, it can be concluded that the AXUV measurement is dominated by the emission of low-medium Ar ionization stages, in line with collisional modelling which suggests that an argon charge state $Z = 11$ is reached after a time of 0.1 ms, see section 4. The deuterium emission is here negligible, as seen from a comparison of Ar doped with non-doped pellets.

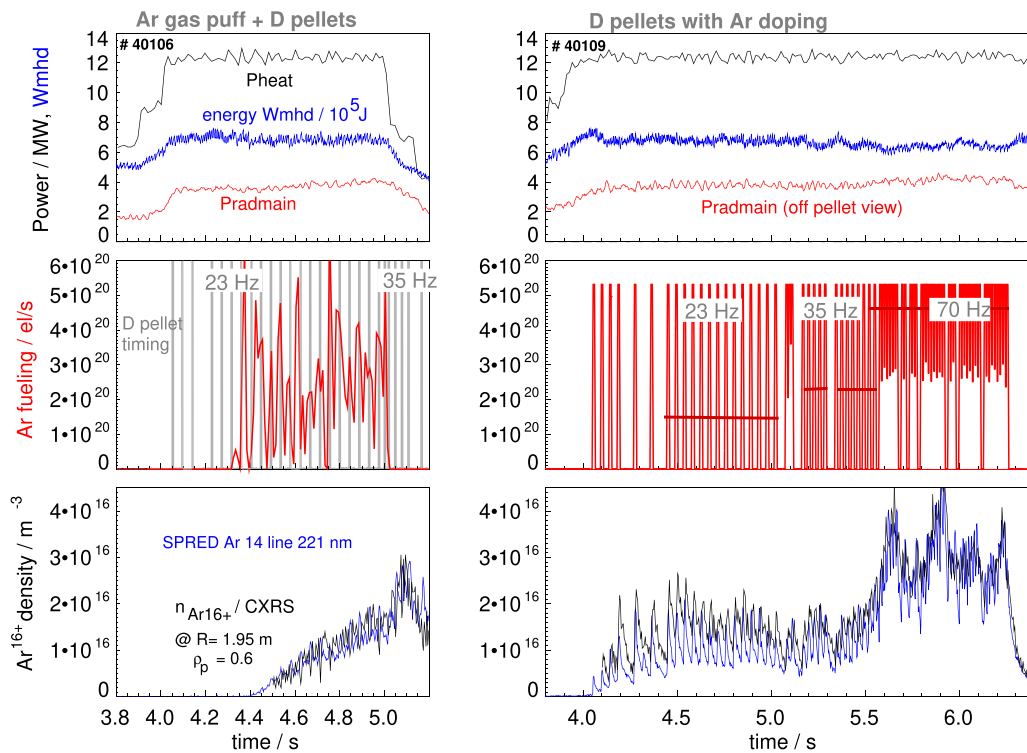


Figure 2. Time traces of two discharges with Ar gas injection from the midplane and pure D pellets (left) and with Ar doped pellets (right). The gas valve modulation is caused by the feedback controller. The Ar fueling by pellets is mimicked in the right figure by normalising the confirmed pellet time stamp in order to obtain the estimated content of 3.6×10^{17} Ar atoms per pellet. Dark red lines indicate the Ar fueling rate at the respective nominal pellet frequency. He-like Ar densities are measured by CXRS [10] and plotted in black for a radial location where this ionization stage is dominant. The blue lines show an Ar¹⁴⁺ VUV line measured by the SPRED spectrometer in relative units. The main chamber radiated power was evaluated from bolometer measurements in a sector toroidally far off the pellet path. $I_p = 1$ MA.

The most important observation is the much higher power emission of the Ar doped pellets compared to otherwise identical pure D pellets. The pellet induced radiation is highly localised around the pellet with some spreading in the parallel field direction as seen from comparison of the DVC and DHC signals in figure 4. The local emission also terminates very quickly after the pellet has passed along, with a time scale of about 20 μ s.

For an estimation of the radiated energy, foil bolometers have to be used. Sightlines 3 and 4 of the F camera (figure 3) cover roughly rectangular geometries and are expected to capture the major fraction of the energy radiated by the pellet. Figure 5 shows the bolometer measurements on identical chords in 5 toroidal positions. Only the chord viewing the pellet directly detects the large immediate emission by the pellet. For the derivation of the absolute power, the apertures of the bolometer chords at the height of the pellet path of $A_3 = 0.046$ m² for chord 3 and $A_4 = 0.0186$ m² for chord 4 have been used, which have been obtained from the diagnostics CAD combined with in-vessel measurements of the geometry. As long as the emission is completely inside the covered area, the power is correctly determined. A moderate under-estimation of the power may be caused by the toroidal extension of the emitting zone being larger than the toroidal viewing width (16 cm for F3 and 10 cm for F4) of the chord. The steep relative decay of the emission measured by toroidally neighboring chords (about 20 cm apart in toroidal

direction) suggests this effect is small. A factor 2 underestimation of the derived radiated energy is regarded as the maximum uncertainty. The strong toroidal localization also suggests that the fast radiation time scale is dominated by low ionized Ar states, since the highest ionization states have such a long ionization time that wide toroidal spreading occurs. The poloidal widths at the unperturbed pellet path are 27 cm and 17 cm for F3 and F4, respectively, giving a good poloidal coverage of the ablating pellet. A typical instantaneous (emitted within a ms) radiated energy of 2.5 kJ is obtained from the sum of the F camera chords 3 and 4. The effect of radiation spreading in toroidal direction outside the view of the bolometer chord would lead to an increased radiated energy.

Clearly, ablation calculations for the doped pellet including modelling of the argon transport around the pellet and its emission and ionisation evolution would be highly desirable. Ablation models for pure neon pellets [14] and neon doped deuterium pellets [15] have recently been developed in view of SPI disruption mitigation experiments. A substantially lower ablation rate and thus a deeper penetration of the pellet is found for a high neon doping fraction of 10% [15]. Interesting questions to a further extended model capable for the treatment of doped pellets and the argon ionization balance and radiation would be the mechanisms determining the radiated energy and its (potentially non-linear) dependence on the doping fraction.

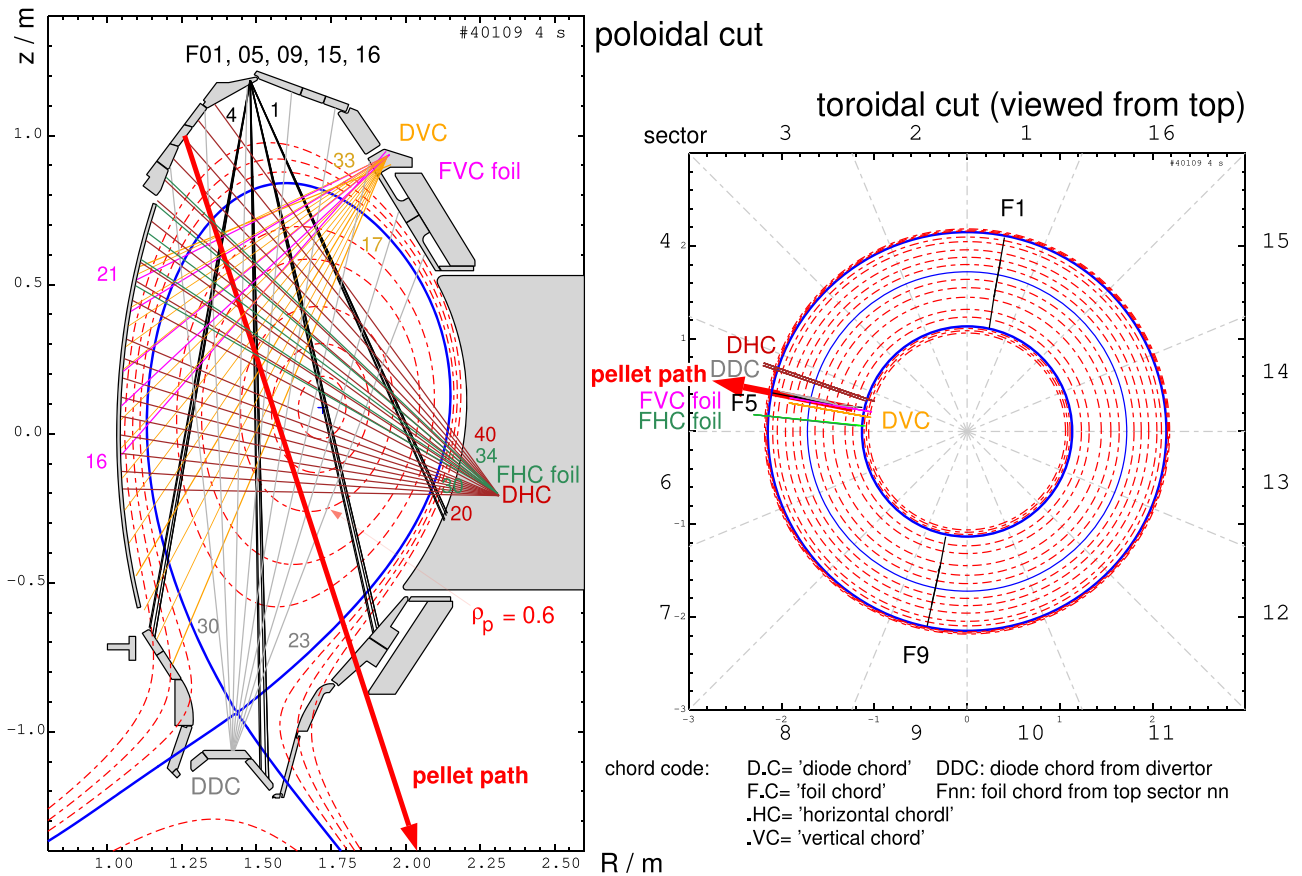


Figure 3. Poloidal and toroidal cuts of the viewing geometry relevant for Ar doped pellet diagnostic with fast, but uncalibrated AXUV diodes (chord names starting with ‘D’) and slow, but calibrated foil bolometers (chord names starting with ‘F’). Chord numbers are indicated beside the shown line of sight bundles. The thick red line is the geometrical pellet path, without drift effects caused by the plasma.

4. Radiation enhancement by deviation from coronal equilibrium

The local release of neutral argon atoms in the outer plasma region during pellet ablation, and their subsequent ionisation leads to increased radiated power compared to the close-to-equilibrium situation obtained by gas fuelling through the SOL. This behavior is seen in the radiative loss function L_z shown in the right plot of figure 6. For decreasing residence time τ , and thus decreasing non-corona parameter $n_e\tau$, the radiative loss function L_z increases in the pedestal temperature range. For the non-coronal ablative pellet conditions, the radiative potential Φ_z [16], shown in the left plot of figure 6, gives a better description compared to the radiative loss function L_z since we are interested in the time-integrated radiated energy. The two quantities are related via $\Phi_z = \tau_z n_e L_z$ [17]. To find out more about the Ar ionization stages which dominate the radiative losses, figure 7 shows the radiated energy and the fractional abundance of different Ar ionization stages in temporal evolution for the case that a neutral Ar atom is put into a plasma with $n_e = 10^{20} \text{ m}^{-3}$ and $T_e = 400 \text{ eV}$. For the corresponding times of 0.1 ms, 0.3 ms and 1 ms the values of the radiative potential from figure 6 for $T_e = 400 \text{ eV}$ are reconciled. The slope of the curve in figure 7 is a measure

for the radiated power. It is high for very low ionization stages, but these do not contribute considerably to the radiated energy due to their short lifetime. From figure 7 and the temporal scale of the measured AXUV emission we infer that the Ar ionization stages which dominate the radiated energy are around Ar^{11+} .

Reading from figure 6 a Φ_z of 10^4 eV for AUG pedestal top conditions at $T_e = 400 \text{ eV}$, the 3.6×10^{17} Ar atoms in a pellet are expected to radiate about 0.6 kJ, or on average 40 kW for a 70 Hz pellet train if only the radiation peak integrated over the pellet ablation time is considered. Φ_z was evaluated using ADAS data [18] for an electron density $n_e = 10^{20} \text{ m}^{-3}$, which is intermediate between the pedestal top electron density ($8 \times 10^{19} \text{ m}^{-3}$) and the central density ($1.3 \times 10^{20} \text{ m}^{-3}$) around $t = 5.5 \text{ s}$. The pellet radiated energy evaluated from atomic data is at least a factor of 4 lower than the 2.5 kJ derived from bolometry, see figure 5. This factor is too large to be covered by uncertainties of bolometry (which could support an underestimation of the derived emitted energy by a factor 2, but the uncertainty of an overestimation is at most 20%). The supposed origin of the higher measured radiation is a stronger deviation from corona equilibrium during the pellet ablation process compared to the ionizing-up calculations assuming constant plasma parameters.

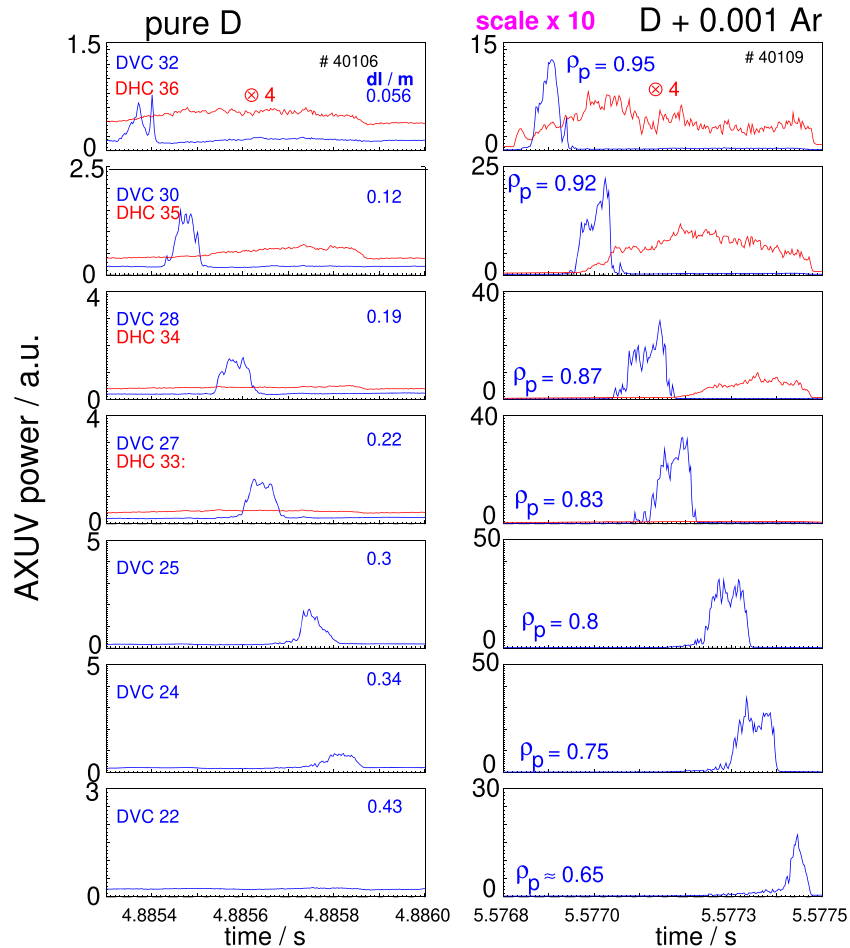


Figure 4. Time dependence of the pellet radiation tracked by different AXUV diodes arranged about perpendicular along the vacuum pellet track, see figure 3. The Ar doped panel, on the right column, exhibits more than an order of magnitude higher radiation compared to a similar pure D pellet, shown on the left column with the scale reduced by the factor 10. The DHC array views about 23 cm away from the pellet path in ctr-current toroidal direction. It is expected to detect higher Ar ionizations stages (Be- to He-like) which are more toroidally distributed due to parallel transport. For the viewing geometry, please see figure 3. dl values shown in the figures denote the distance to the separatrix measured along the vacuum pellet path of the crossing point of the respective viewing lines with the vacuum pellet path, ρ_p is the crossing ρ_{poloidal} of the viewing line with the pellet path. Plotting scales were adapted for appropriateness to the much lower emission of the undoped pellet on the DHC array.

This deviation may be caused by plasma parameter variations very close to the pellet, leading to a rise of the radiative potential (see figure 6). Another potentially very positive effect deserves attention: the Ar radiative losses may be further enhanced by the presence of deuterium neutrals [19] ablated from the pellet, which reduce the ionization degree of Ar by charge exchange below its equilibrium value, and thus leading to radiation enhancement. In the case of doped deuterium pellets, the pellet released D neutrals are expected to at least locally dominate those resulting from fueling and wall recycling. The pellet released neutrals can effect the short radiation peak during ionising-up as well as the emissivity of the underlying, steady Ar content. It should be noted that the enhancement of the Ar radiation by neutrals has been found from Li-like ($Z = 15$) down to at

least Mg-like ($Z = 6$) argon [19]. The higher charge states are expected to be more toroidally distributed, and probably the origin of the radiation seen in the DHC channels 23 cm away from the pellets shown in figure 4. In summary, a detailed modelling of the Ar doped pellet ablation process including the ionisation and excitation of Ar will be required for a quantitative reproduction of the experimental results. The factor 4 underestimation of the emission by the simple model, and the likely presence of further non-corona enhancement effects are a good starting point. If these effects can be quantified, and predicted to be still present for reactor conditions, impurity doped pellets may allow for more efficient plasma cooling (in terms of Z_{eff} rise per radiated power) in the pedestal region, combined with faster response times.

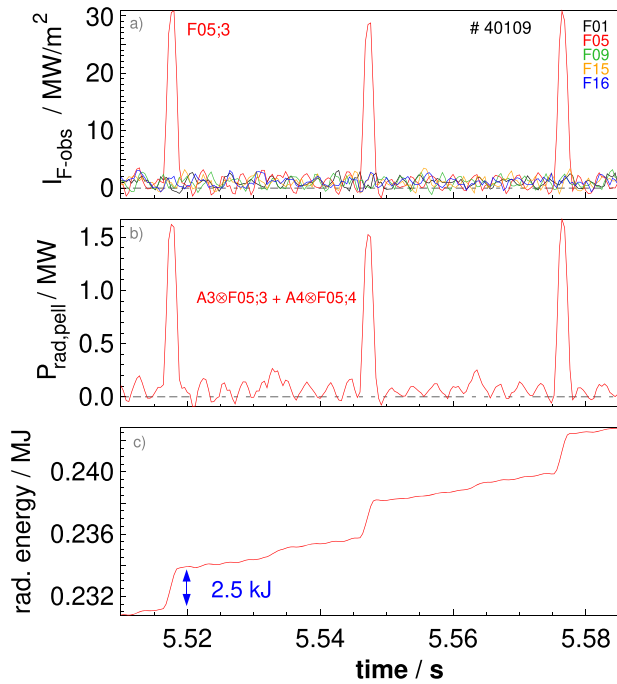


Figure 5. Pellet emitted energy derived from foil bolometry. (a) Line integrated brightness from F chords number 3 viewing from the top in 5 toroidal positions. (b) Sum of the emitted power from chords 3 + 4 by multiplication of the power densities with the viewed area A at the crossing of viewing line and pellet path. (c) Radiated energy from time integration of (b), with the steps corresponding to the pellet ablation. A typical radiated energy of 2.5 kJ is obtained per pellet containing 3.6×10^{17} Ar atoms. Note that foil bolometry has been evaluated with faster than standard time resolution.

5. Ar-doped pellets sustain no-ELM conditions in QCE H-mode

The question arises whether Ar doped pellet injection is compatible with no-ELM scenarios for AUG conditions. Pellet fuelling in a no-ELM scenario should not trigger ELMs. We use here a quasi-continuous exhaust (QCE) H-mode, where type-I ELMs are suppressed by pedestal tailoring at high plasma shaping [20, 21]. Figure 8 compares a no-ELM QCE H-mode discharge with the ELMy H-mode discharge discussed before. Both discharges use the same setup for Ar doped pellets. The QCE scenario # 40313 has a lower plasma current compared to the standard H-mode # 40109 (0.8 MA compared to 1 MA), but a higher shaping (upper triangularity 0.32 compared to 0.1), and slightly lower heating power. During the maximum pellet frequency phase, the pedestal top electron density is slightly higher in QCE (10 versus $9 \times 10^{19} \text{ m}^{-3}$), while the pedestal temperature around $\rho_{pol} = 0.95$ is lower (300 eV compared to 450 eV). While in the ELMy discharges, ELMs are triggered by the pellet if enough time has elapsed after the previous ELM [7], no ELM triggering occurs in the QCE discharge, including the first pellets, for which the pedestal top has still a lower density. The energy radiated by each pellet is similar in both discharges.

6. Discussion and conclusions

The injection of argon-doped deuterium pellets into ASDEX Upgrade H-mode discharges allows for a fast and intense rise of the plasma radiation in the pedestal region. The radiation released during pellet ablation may be beneficial for fast control tasks, e.g. during divertor re-attachment, and provide an increased overall radiation efficiency. After a short time scale of about 0.1 ms during pellet ablation (at one spatial position, the whole ablation along the pellet path lasts about 0.6–0.8 ms) with a very high, but localised radiation level, toroidally symmetric enhanced radiation is observed with an e-folding decay time of about 20 ms related to Ar transport. After this time, Ar recycling and pumping takes place very similar to that observed in a gas-puff case, with a pumping time scale of 200 ms as measured after the stop of the pellet injection. The Ar radiation during pellet ablation reveals an increased radiation level compared to that observed for gas puffing, which allows a more efficient radiative pedestal cooling in terms of radiation per fuel dilution. A simple non-coronal model using the radiative potential of Ar falls at least a factor of 4 short in comparison to the measured radiative energy, therefore additional effects during ablation must play a role which still have to be identified. Injection of Ar doped pellets into an QCE H-mode discharge revealed compatibility with the no-ELM conditions in ASDEX Upgrade, since no ELM triggering occurred.

Due to the localization of the pellet-induced radiation, a full application of the doped pellet scheme may require a number of toroidally distributed injectors. For DEMO, a set of about ten injectors can be imagined, ideally with real-time selection between different fuel/impurity mixtures in each injector. A much higher dopant concentration compared to the present AUG experiments has to be used to obtain a sufficient radiative cooling. For example, assuming ten injectors with 100 Hz and 2% Ar concentration, 50 MW radiation by immediate ablation would be obtained from simple up-scaling of AUG with identical pellet size. Krypton and xenon [4] should be considered as additional pellet doping species for a further radiation increase.

While the faster reaction time in comparison to gas puffing is a clear advantage, the question arises to what extent a higher radiative efficiency can be achieved under stationary conditions. To answer this question, we compare the immediate radiative power within the ablation with the radiated power associated with the recycling argon. For ASDEX Upgrade during 35 Hz pellet injection, we obtain a time-averaged Ar density of $1.5 \times 10^{16} \text{ m}^{-3}$ connected to a direct radiated power during the fast ionizing process of $35 \text{ 1/s} \times 2.5 \text{ kJ} = 88 \text{ kW}$. The radiated power rise associated to argon in the comparison shot with gas puffing and similar Ar concentration cannot be reliably determined due the weak rise of the radiation and the change of plasma parameters due to the density rise caused by the pellets. Scaling down from similar shots with a higher argon puff rate and no pellet injection suggest a recycling radiation rise by the pellet injected argon of about 200 kW.

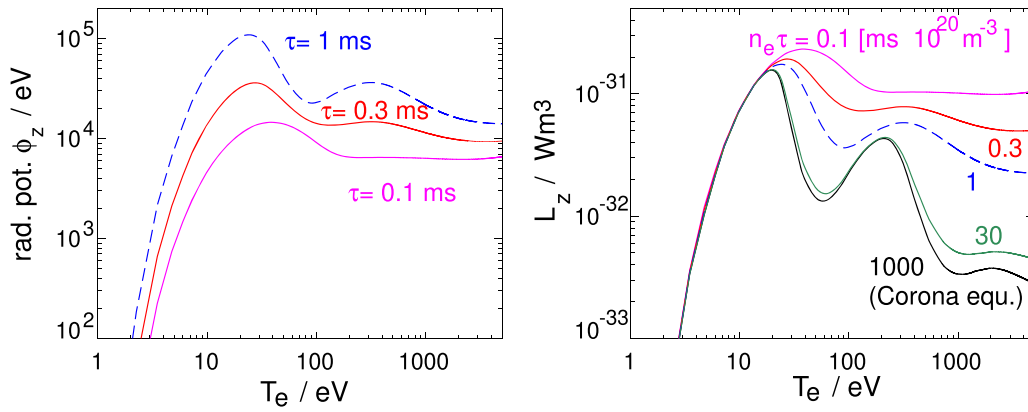


Figure 6. Radiative potential Φ_z and radiative loss function L_z of argon for different residence times τ_z and an electron density of 10^{20} m^{-3} . Φ_z gives the energy radiated by a neutral Ar atom if resident under the given plasma parameters for the time τ .

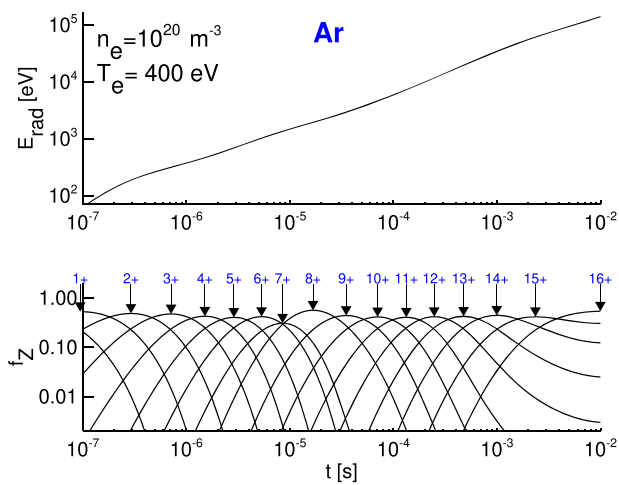


Figure 7. Temporal development of the time-integrated radiated energy by an argon atom put into a plasma with $n_e = 10^{20} \text{ m}^{-3}$ and $T_e = 400 \text{ eV}$. The values at the different times correspond to the radiative potential at the corresponding values of τ , see figure 6. Also shown are the fractional abundances of the different Ar ionization stages during the course of the ionization process up to helium-like argon.

This means that the immediate radiation during ablation adds up 40%–50% to the main plasma radiation expected from the same argon concentration produced by gas puffing. For a DEMO-type device, the additional contribution by the power emitted during ablation is expected to be lower on the relative scale since the residence time of argon will be longer compared to AUG. However, a beneficial effect of the argon source being situated in the pedestal gradient region is expected in DEMO due to the neoclassical outward drift at conditions of high pedestal ion temperature [23]. The impurity doping scheme

would have to be integrated into the complete DEMO fuel cycle, which includes plasma enhancement gases like argon [24, 25], and into the overall impurity seeding strategy [3, 26]. Fast Ar pumping will help to reduce the less efficient radiation contribution related to Ar recycling, thus maximizing $\delta P_{\text{rad}}/\delta Z_{\text{eff}}$.

The proposed scheme offers prospects for an efficient radiative cooling under stationary conditions as well as a quick reaction on transient re-attachment on a short timescale. The ASDEX Upgrade doped pellet scheme is currently limited in the maximum concentration of the dopant. This is due to a change in mechanical properties of the ice, which may cause damage to the stop cylinder of the pellet injection system. Installation of an adapted stop cylinder will allow to overcome this problem. Finally, pellet ablation calculations [14, 15] for doped conditions would be highly desirable. These should include collisional-radiative modelling of the doped impurity, including possible effects of charge exchange of impurity ions with neutral fuel atoms. A first application of such a model would be to check whether the expected radiation scales linearly with the number of argon atoms, as assumed in our simple model.

Acknowledgments

This work has been carried out within the framework of the EUROfusion Consortium, funded by the European Union via the Euratom Research and Training Programme (Grant Agreement No. 101052200—EUROfusion). Views and opinions expressed are however those of the author(s) only and do not necessarily reflect those of the European Union or the European Commission. Neither the European Union nor the European Commission can be held responsible for them.

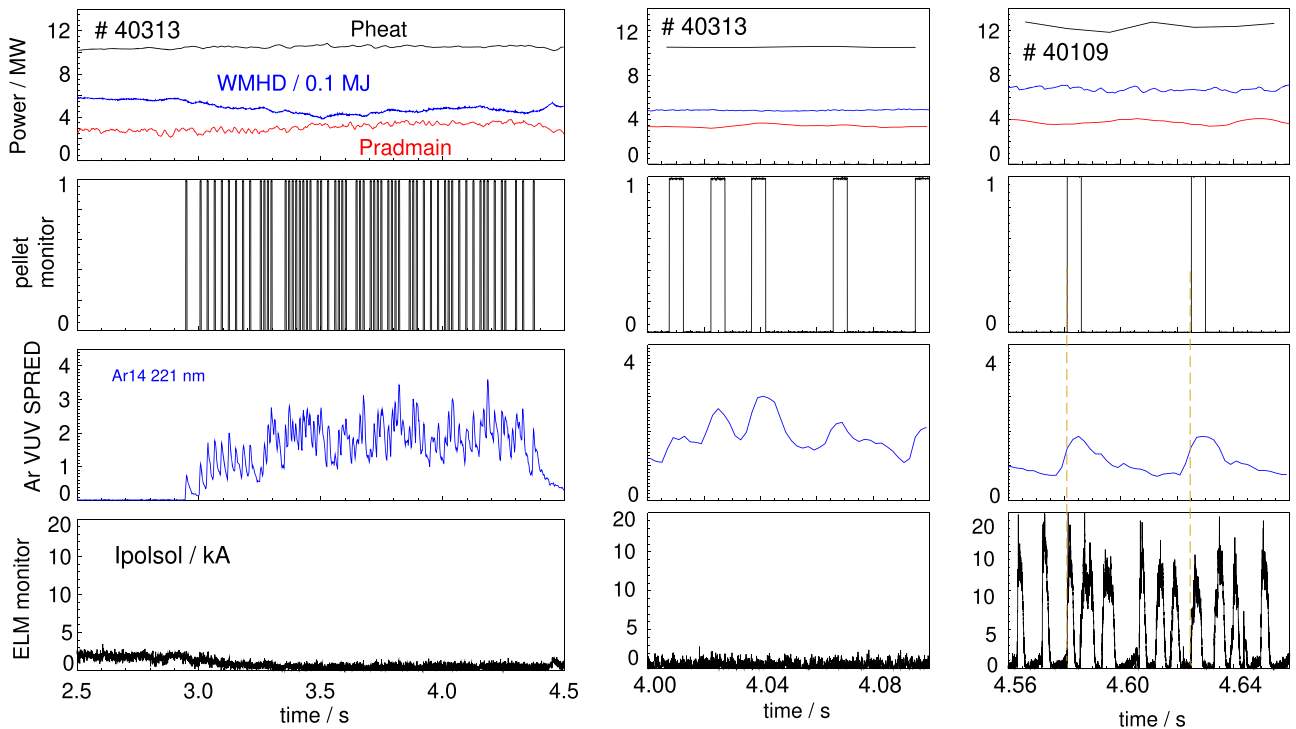


Figure 8. Ar doped pellet injection into a no-ELM QCE H-mode discharge # 40313, $I_p = 0.8$ MA. The no-ELM state is preserved, no triggering of ELMs is observed by the pellets. For a better temporal resolution, 100 ms time intervals of the discharge are compared to the ELMy discharge # 40109, see figure 2. The poloidal current into the target measured by shunts is used as ELM monitor, this quantity is a proxy for the heat flux [22].

ORCID iDs

A. Kallenbach <https://orcid.org/0000-0003-0538-2493>
 R.M. McDermott <https://orcid.org/0000-0002-8958-8714>
 B. Ploeckl <https://orcid.org/0000-0001-6057-5402>
 A. Zito <https://orcid.org/0000-0002-6743-6568>

References

- [1] Kallenbach A. et al (ASDEX Upgrade Team and EUROfusion MST Team) 2021 *Nucl. Fusion* **61** 016002
- [2] Pitts R.A. et al 2019 *Nucl. Mater. Energy* **20** 100696
- [3] Siccino M., Federici G., Kembleton R., Lux H., Maviglia F. and Morris J. 2019 *Nucl. Fusion* **59** 106026
- [4] Lang P.T. et al 2021 *Fusion Sci. Technol.* **77** 42
- [5] Lang P.T. et al 2018 *Nucl. Fusion* **58** 036001
- [6] Lang P.T. et al 2019 *Nucl. Fusion* **59** 026003
- [7] Lang P.T. et al 2014 *Nucl. Fusion* **54** 083009
- [8] Kallenbach A., Bernert M., Eich T., Fuchs J.C., Giannone L., Herrmann A., Schweinzer J. and Treutterer W. 2012 *Nucl. Fusion* **52** 122003
- [9] Kallenbach A. et al 2021 *Nucl. Fusion* **61** 016002
- [10] McDermott R.M., Dux R., Guzman F., Pütterich T., Fischer R. and Kappatou A. 2021 *Nucl. Fusion* **61** 016019
- [11] Bernert M., Eich T., Burckhart A., Fuchs J.C., Giannone L., Kallenbach A., McDermott R.M. and Sieglin B. 2014 *Rev. Sci. Instrum.* **85** 033503
- [12] Müller H.W., Dux R., Kaufmann M., Lang T., Lorenz A., Maraschek M., Mertens V. and Neuhauser J. (ASDEX Upgrade Team) 2002 *Nucl. Fusion* **42** 301
- [13] Kocsis G., Kálvin R., Veres G., Cierpka P., Lang P.T., Neuhauser J. and Wittman C. (ASDEX Upgrade Team) 2004 *Rev. Sci. Instrum.* **75** 4754
- [14] Bosviel N., Parks P. and Samulyak R. 2021 *Phys. Plasmas* **28** 012506
- [15] Matsuyama A. 2022 *Phys. Plasmas* **29** 042501
- [16] Samm U. et al 1990 *J. Nucl. Mater.* **176–177** 273
- [17] Kallenbach A., Bernert M., Dux R., Eich T., Henderson S.S., Pütterich T., Reimold F., Rohde V. and Sun H.J. 2019 *Nucl. Mater. Energy* **18** 166
- [18] 2022 The ADAS project (<https://adas.ac.uk/documentation.php>)
- [19] Dux R., Cavedon M., Kallenbach A., McDermott R.M. and Vogel G. (The ASDEX Upgrade Team) 2020 *Nucl. Fusion* **60** 126039
- [20] Harrer G.F. et al 2018 *Nucl. Fusion* **58** 112001
- [21] Faitsch M., Eich T., Harrer G.F., Wolfrum E., Brida D., David P., Griener M. and Stroth U. 2021 *Nucl. Mater. Energy* **26** 100890
- [22] Kallenbach A. et al 2010 *Plasma Phys. Control. Fusion* **52** 055002
- [23] Dux R. et al 2014 *Plasma Phys. Control. Fusion* **56** 124003
- [24] Abdou M., Riva M., Ying A., Day C., Loarte A., Baylor L.R., Humrickhouse P., Fuerst T.F. and Cho S. 2021 *Nucl. Fusion* **61** 013001
- [25] Day C. et al 2022 *Fusion Eng. Des.* **179** 113139
- [26] Subba F., Coster D.P., Moscheni M. and Siccino M. 2021 *Nucl. Fusion* **61** 106013